Personalized Patch-Based Normality Assessment of Brain Atrophy in Alzheimer's Disease

Jianwei Zhang[1,2] and Yonggang Shi[1,2(✉)]

[1] Stevens Neuroimaging and Informatics Institute, Keck School of Medicine, University of Southern California (USC), Los Angeles, CA 90033, USA
yonggans@usc.edu

[2] Ming Hsieh Department of Electrical and Computer Engineering, Viterbi School of Engineering, University of Southern California (USC), Los Angeles, CA 90089, USA

Abstract. Cortical thickness is an important biomarker associated with gray matter atrophy in neurodegenerative diseases. In order to conduct meaningful comparisons of cortical thickness between different subjects, it is imperative to establish correspondence among surface meshes. Conventional methods achieve this by projecting surface onto canonical domains such as the unit sphere or averaging feature values in anatomical regions of interest (ROIs). However, due to the natural variability in cortical topography, perfect anatomically meaningful one-to-one mapping can be hardly achieved and the practice of averaging leads to the loss of detailed information. For example, two subjects may have different number of gyral structures in the same region, and thus mapping can result in gyral/sulcal mismatch which introduces noise and averaging in detailed local information loss. Therefore, it is necessary to develop new method that can overcome these intrinsic problems to construct more meaningful comparison for atrophy detection. To address these limitations, we propose a novel personalized patch-based method to improve cortical thickness comparison across subjects. Our model segments the brain surface into patches based on gyral and sulcal structures to reduce mismatches in mapping method while still preserving detailed topological information which is potentially discarded in averaging. Moreover, the personalized templates for each patch account for the variability of folding patterns, as not all subjects are comparable. Finally, through normality assessment experiments, we demonstrate that our model performs better than standard spherical registration in detecting atrophy in patients with mild cognitive impairment (MCI) and Alzheimer's disease (AD).

Keywords: Personalized Atlas · Alzheimer's disease · Shape Analysis

1 Introduction

Neurodegenerative diseases like Alzheimer's disease (AD) are the main causes of cognitive impairment and earlier neuropathological alterations [7]. Cortical

Y. Shi—This work is supported by the National Institute of Health (NIH) under grants R01EB022744, RF1AG077578, RF1AG056573, RF1AG064584, R21AG064776, P41EB015922, U19AG078109.

H. Greenspan et al. (Eds.): MICCAI 2023, LNCS 14224, pp. 55–62, 2023.
https://doi.org/10.1007/978-3-031-43904-9_6

thickness change is an essential feature that can quantify the potential brain atrophy in these diseases [9,12]. To analyze cortical thickness across different subjects, one essential step is to find the correspondence between surface points for thickness analysis [14,15]. This is traditionally achieved through 1-to-1 mapping or averaging feature in the region of interest (ROI). Mapping methods typically rely on surface registration techniques on a canonical space such as the unit sphere or high-dimensional embedding space [5,6,10].However,surface registration methods have limitations in accounting for the intrinsic variations in cortical topography among different individuals. For instance, a one-to-one mapping using surface registration could wrongly map a gyral region into a sulcal region due to distinguished local topography between subjects,as example shown in Fig. 1(B), thereby introducing noise into cortical thickness analysis since gyral and sulcal regions have distinct thickness profiles,as example shown in Fig. 1(A). Alternatively, ROI-based methodologies rely on the correspondence of anatomically segmented ROIs and establish comparisons through mean feature extraction. This approach disregards intra-ROI variability and the averaging process obscures detailed folding patterns. To mitigate the inherent challenges of surface mapping and mean ROI feature extraction, novel methodologies that consider the variability in folding patterns for identifying correspondences across distinct topographies are imperative.

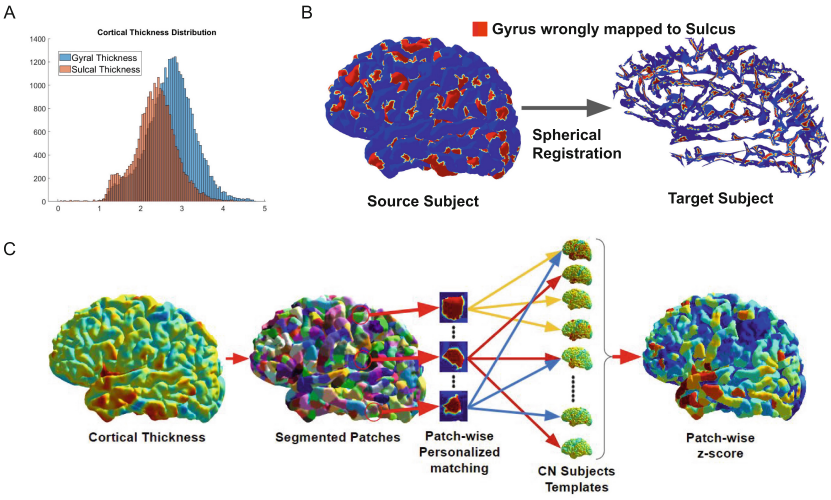

Fig. 1. (A) The plot shows the distinct cortical thickness distributions of gyral/sulcal regions. (B) From gyral/sulca segmentation [13], the red parts of the left plot highlight the mismatched gyral region to sulcal region. The right plot displays mismatched sulcal region. (C) The diagram covers the process of personalized matching, where cortical surface is segmented into small patches and matched onto its own personalized set of templates for normality assessment using z-score.

In this paper, we propose a novel personalized patch-based folding analysis method that finds correspondence through segmented patch similarity and personalized template set. Comparing to conventional methods, our method accounts for the gyral/sulcal mismatch problem by explicitly matching gyral and sulcal patches to their respective regions and selecting a personalized set of templates for each patch, as shown in Fig. 1(C), such that only comparable features are measured together to increase sensitivity in brain atrophy detection and reduce noise introduced by mismatching.

2 Methods

In this section, we will present the technical details of our method, which involve three main parts: surface segmentation, similarity metric and personalized templates. By integrating these 3 parts, we demonstrate the effectiveness of our method through normality assessment experiments on patients with mild cognitive impairment (MCI) and Alzheimer's disease (AD) on data from Alzheimer Disease Neuroimaging Initiative(ADNI) [11].

2.1 Brain Surface Segmentation

We employ FreeSurfer to extract 3D surface mesh from T1-weighted Volumetric MRI data. [2]. We extracted both pial and white surfaces, which have vertex correspondence by reconstruction method. The meshes are decimated to 50000 vertices for computational cost. The brain mesh is then subdivided into gyral and sulcal sub meshes following the methods in [13] using shape index and graph cut. The intricate folding pattern of the brain's cortical surface can make it difficult to accurately classify certain gyral structures that extend deeper from the outer surface. However, these structures can be better detected on the white surface, which has more prominent gyrus. Therefore, the segmentations from pial and white surfaces are combined through vertex correspondence. Specifically, given two array $mask_p$ and $mask_w$ as segmentation mask from pial and white surfaces, the final mask is $mask_p|mask_w$, where entry 1 is gyrus and 0 is sulcus. The resulting gyral/sulcal surfaces are 3D meshes with disconnected components and boundaries due to noise in reconstruction and the intrinsic geometry of the folding pattern. Therefore, filtering is applied to eliminate components that have less vertices than a threshold, which is empirically set at 50.

The segmented patches are generated for gyral and sulcal sub meshes separately, which is shown in Fig. 2(B). Given a 3d mesh $M(V, F)$, V as set of vertices and F as set of faces, the boundary of M is defined as $B(M)$, the set of vertices that has at least one neighboring edge that is contained in only one triangular face. Next, the distance transform of vertex $v \in V$ is defined as:

$$DT(v) = \min_{b \in B(M)} Geo(v, b) \tag{1}$$

The Geo denotes the geodesic distance between v and b. The distance transform computation is implemented using fast marching algorithm. [8] From the distance

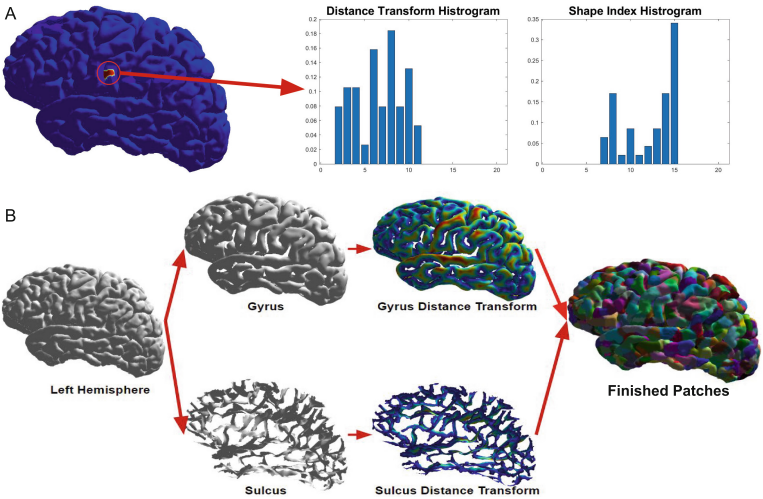

Fig. 2. (A) Example of segmented patch and its histogram shape descriptor (B) Process of the segmentation, from gyral/sulcal segmentation, distance transform computation to patch generation

transform, we can obtain a set L of local maximum vertices, defined as $\{v \in V : DT(v) >= DT(w), \forall w \in Neighbor(w)\}$. The neighbors of a vertex v is the set of vertices that connect to v by one edge. With L and Geo, we can compute the Voronoi diagram that consists of Voronoi cells defined as:

$$C_i = \{x \in V : Geo(x, c_i) <= Geo(x, c_j); \forall c_j \in L\} \tag{2}$$

Each Voronoi cell defines a segmented patch. Since the surface is not perfectly smooth, the mesh is usually over segmented. To address this issue, we employ a region grow strategy to merge patches. Starting from one patch, we compute the geodesic distances between its center vertex and those of all neighboring patches. If the computed distance falls below a specified threshold, the two patches are merged into a single patch. In the event that no neighboring patch meets this criterion, we proceed to an unvisited patch. The iteration repeats until all patches are visited. The threshold is empirically set as twice the mean edge length on the mesh. Patches are labeled as gyral or sulcal based on the sub-mesh they're generated from.

2.2 Patch Similarity Metric

We employ shape similarity metrics to identify comparable patches. Histogram-based shape descriptors are used for topological similarity. Specifically, a histogram H is constructed for a function F defined on all vertices in a patch. The input values for histogram generation are normalized by the root mean square (RMS) of the function. The maximum bin value of the histogram is set as the

maximum feature value, and the number of bins is fixed at 20 to ensure comparability between histograms. The values in each bin are normalized with respect to the total number of vertices in the patch, ensuring that the histogram values add up to 1. This normalization is done to avoid the scaling problem, as patches with similar topography can have different sizes. The distance transform, described in previous section, and shape index are used for constructing histogram, H_{dt} and H_{si}. Distance transform is used since the distance to boundary encodes information about the gyral/sulcal patches,such as width of the gyrus. For example, a crest gyral structure and a plateau one have different distance to boundary distribution. For topological comparison, chi square distance is computed as similarity. Given histograms H_i and H_j, the chi square distance is defined below:

$$D_{\chi 2}(H_i, H_j) = \Sigma_k \frac{(H_i[k] - H_j[k])^2}{H_i[k] + H_j[k]} \tag{3}$$

$H_i[k]$ denotes the value in the kth bin of H_i. For any two patches,i and j, we can define a distance vector $v_{dist}(i,j) = [D_{\chi 2}(H_i^{dt}, H_j^{dt}), D_{\chi 2}(H_i^{si}, H_j^{si}), D(C_i, C_j)]$. The final similarity score $S(i,j)$ is defined as $\frac{1}{||w \times v_{dist}(i,j)||}$, where w is a weighting vector.

2.3 Personalized Template Set

To mitigate the impact of inter-subject variability in brain structure folding patterns, a personalized set of templates is chosen for each patch. This involves selecting a cohort of N cognitively normal (CN) subjects as the templates for comparison, while a separate group of M mild cognitive impairment (MCI) and M Alzheimer's disease (AD) subjects is selected for testing purposes.

For all subjects in both the template and test groups, we first obtain the sets T_{temp} and T_{test} of segmented patches as described in the previous section. From the output of Freesurfer, we compute the vertex-wise spherical registered coordinates (stored in the sphere.reg file) and cortical thickness (stored in the .thickness file) as $SR(v)$ and $CT(v)$, respectively, where v denotes a vertex [4]. For a query patch P_i, which is a set of vertices and has a gyral/sulcal label from the sub mesh they are generated from, we first compute its patch spherical registered coordinates $PSR_i = \frac{1}{|P_i|} \sum_{v \in P_i} SR(v)$ and patch cortical thickness $PCT_i = \frac{1}{|P_i|} \sum_{v \in P_i} CT(v)$, where $|P_i|$ is the cardinality of P_i. Then, for each patch $P_i \in T_{test}$, we compute the nearest 200 patches $P^{1\ldots200} \subset T_{temp}$ that has the same gyral/sulcal label as query patch in terms of $||PSR_i - PSR_j||$, where $P_j \in T_{test}$. This is to leverage the location information of the patch with respect to the whole hemisphere, as matched patches should be from the neighborhood region of the query patch and label restriction is to reduce mismatch of gyral/sulcal regions. From $P^{1\ldots200}$, we select the 50 most similar patches based on their similarity scores. Specifically, we compute the similarity score $S(i,j)$ for patch P_i and patch $P_j \in P^{1\ldots200}$, and choose the top 50 patches in $P^{1\ldots200}$ with the largest similarity scores to form a personalized template set T_{P_i} for patch P_i. We repeat this process for each patch in the test set.

In the next step, we define the normality metric used to measure the normality of a patch. For each patch P_i and its personalized template set T_{P_i}, we first compute the mean (μ) and standard deviation (std) of the patch cortical thickness for all patches in T_{P_i}. We then define the z-score of P_i as $Z(P_i) = |\frac{PCT_{p_i} - \mu}{std}|$. This z-score is used as a normality measure because if P_i is abnormal, it will have a larger z-score and vice versa. Finally, we use this z-score for each patch in the test subject set to conduct normality assessment experiments.

3 Results

3.1 Normality Assessment Experiments

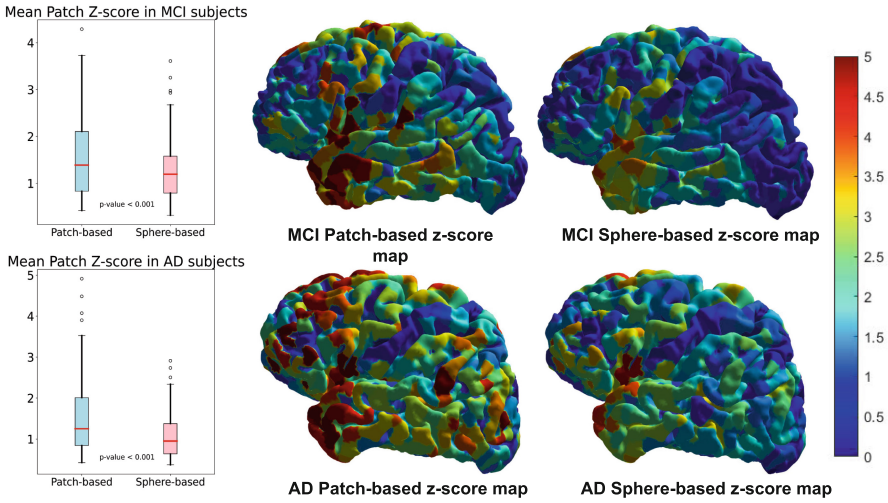

Fig. 3. The Left 2 plots show the results of normality assessment experiment. The right 4 plots show the visualization of patch-based and sphere-based z-score map on MCI and AD subjects

To investigate the discriminative power of our patch-based personalized matching approach, we randomly selected 200 cognitive normal (CN) subjects as templates, 100 mild cognitive impairment (MCI) and 100 Alzheimer's disease (AD) subjects from the ADNI dataset to compare our method to Freesurfer's Spherical Registration. The experiments are limited to the left hemisphere for computing cost. Specifically, we used the sphere.reg file output from Freesurfer, which was decimated to 50000 vertices. For each query subject's surface, we computed the spherical registration of each vertex to a template surface by finding the closest vertex in the template's vertices based on Euclidean distance on the unit sphere space, as described by the sphere.reg file. We then computed a patch-based z-score for each patch P_i using the thickness of P_i and the spherically matched

vertices from each template subject, which we denote as the sphere-based z-score. Alternatively, we matched patches as previously described in the Method section, and computed a patch-based z-score for each patch in the MCI and AD subject sets.

For each MCI and AD subject, the mean sphere-based z-score and mean patch-based z-score are computed by averaging the respective scores of patches for 1 subject. These mean z-scores represent how abnormal a subject is. The resulting distributions are shown in Fig. 3. The results show that our method yields a higher z-score for MCI and AD subjects compared to the sphere-based z-score, indicating that our model is more sensitive in detecting brain atrophy. As a qualitative analysis, the patch-based z-score maps and sphere-based z-score maps for selected MCI and AD subjects are also shown in Fig. 3. The patch-based z-score map shows more brain atrophy than the sphere-based z-score map, which further verifies our model's advantage in brain atrophy detection.

3.2 CN vs MCI, AD Prediction Experiment

In this experiment, we conduct CN vs MCI and CN vs AD prediction accuracy test. Similar to previous experiment, we choose 200 CN subjects as templates and another 100 CN subjects, 100 MCI subjects and 100 AD subjects for testing. Afterwards, sphere-based z-scores and patch-based z-scores are computed for all patches in CN, MCI and AD subjects from 200 template subjects. For training feature, we use the mean z-score of patches in each ROI in one subject, which is a length-34 vector for 34 ROIs from Freesurfer(*.aparc.annot*) [3]. Each subject has one feature vector generated from patch-based z-score and one from sphere-based z-score. The CN, MCI and AD are used as labels. The feature vectors and labels are randomly split into train and test set at 8:2 ratio. The classifier we use is a generic support vector machine from sklearn package [1]. The test is conducted for CN vs AD and CN vs MCI binary classifications. We used 5-fold cross validation for evaluation on stability. The resulting test accuracy is shown in Table 1. The results show that our method performs better in accuracy than sphere-based method.

Table 1. test accuracy for CN vs AD and CN vs MCI

Feature Type	CN vs. AD Accuracy(%)	CN vs. MCI Accuracy(%)
Sphere-based	68.33	50.84
Patch-based	**71.66**	**58.50**

4 Conclusion

In this paper, we proposed a novel personalized patch-based method for brain atrophy detection by matching segmented patches based on gyral/sulcal label,

location, shape similarity and constructing personalized template set for abnormal detection. Through normality assessment and MCI AD prediction experiments, the method is shown to be more effective at detecting brain atrophy.

References

1. Buitinck, L., et al.: API design for machine learning software: experiences from the scikit-learn project. In: ECML PKDD Workshop: Languages for Data Mining and Machine Learning, pp. 108–122 (2013)
2. Dale, A.M., Fischl, B., Sereno, M.I.: Cortical surface-based analysis: I. segmentation and surface reconstruction. NeuroImage **9**(2), 179–194 (1999)
3. Fischl, B., et al.: Automatically parcellating the human cerebral cortex. Cereb. Cortex **14**(1), 11–22 (2004)
4. Fischl, B., Sereno, M.I., Tootell, R.B., Dale, A.M.: High-resolution intersubject averaging and a coordinate system for the cortical surface. Hum. Brain Mapp. **8**(4), 272–284 (1999)
5. Gahm, J.K., Shi, Y.: Riemannian metric optimization on surfaces (RMOS) for intrinsic brain mapping in the Laplace-Beltrami embedding space. Med. Image Anal. **46**, 189–201 (2018)
6. Gu, X., Wang, Y., Chan, T., Thompson, P., Yau, S.T.: Genus zero surface conformal mapping and its application to brain surface mapping. IEEE Trans. Med. Imaging **23**(8), 949–958 (2004)
7. Jack, C.R., Jr., et al.: NIA-AA research framework: toward a biological definition of Alzheimer's disease. Alzheimer's Dement. **14**(4), 535–562 (2018)
8. Kimmel, R., Sethian, J.A.: Computing geodesic paths on manifolds. Proc. Natl. Acad. Sci. **95**(15), 8431–8435 (1998)
9. Lerch, J.P., Pruessner, J.C., Zijdenbos, A., Hampel, H., Teipel, S.J., Evans, A.C.: Focal decline of cortical thickness in Alzheimer's disease identified by computational neuroanatomy. Cereb. Cortex **15**(7), 995–1001 (2004)
10. Lyu, I., Kang, H., Woodward, N., Styner, M., Landman, B.: Hierarchical spherical deformation for cortical surface registration. Med. Image Anal. **57** (2019)
11. Mueller, S.G., et al.: The Alzheimer's disease neuroimaging initiative. Neuroimaging Clin. North Am. **15**(4), 869–877 (2005). Alzheimer's Disease: 100 Years of Progress
12. Querbes, O., et al.: Early diagnosis of Alzheimers disease using cortical thickness: impact of cognitive reserve. Brain: J. Neurol. **132**, 2036–47 (2009)
13. Shi, Y., Thompson, P.M., Dinov, I., Toga, A.W.: Hamilton-Jacobi skeleton on cortical surfaces. IEEE Trans. Med. Imaging **27**(5), 664–673 (2008)
14. Thompson, P.M., et al.: Mapping hippocampal and ventricular change in Alzheimer disease. Neuroimage **22**(4), 1754–1766 (2004)
15. Thompson, P.M., et al.: Mapping cortical change in Alzheimer's disease, brain development, and schizophrenia. Neuroimage **23**, S2–S18 (2004)